Environmental Science & Technology

Article

pubs.acs.org/est

High-Resolution Remote Sensing of Water Quality in the San Francisco Bay–Delta Estuary

Cédric G. Fichot,*[,†] Bryan D. Downing,[‡] Brian A. Bergamaschi,[‡] Lisamarie Windham-Myers,[§] Mark Marvin-DiPasquale,[§] David R. Thompson,[†] and Michelle M. Gierach[†]

[†]Jet Propulsion Laboratory, California Institute of Technology, Pasadena, California 91109, United States

[‡]United States Geological Survey, Sacramento, California 95819, United States

[§]United States Geological Survey, Menlo Park, California 94025, United States

Supporting Information

ABSTRACT: The San Francisco Bay–Delta Estuary watershed is a major source of freshwater for California and a profoundly human-impacted environment. The water quality monitoring that is critical to the management of this important water resource and ecosystem relies primarily on a system of fixed water-quality monitoring stations, but the limited spatial coverage often hinders understanding. Here, we show how the latest technology in visible/near-infrared imaging spectroscopy can facilitate water quality monitoring in this highly dynamic and heterogeneous system by enabling simultaneous depictions of several water quality indicators at very high spatial resolution. The airborne portable remote imaging spectrometer (PRISM) was used to derive high-spatial-resolution (2.6 × 2.6 m) distributions of turbidity, and dissolved organic carbon (DOC) and chlorophyll-a concentrations in a wetland-influenced region of this estuary. A filter-passing methylmercury vs DOC relationship was also developed using in situ samples and enabled the high-spatial-resolution depiction of surface methylmercury concentrations in this area. The results illustrate how high-resolution imaging spectroscopy can inform management and policy development in important inland and estuarine water bodies by facilitating the detection of point- and nonpoint-source pollution, and by providing data to help assess the complex impacts of wetland restoration and climate change on water quality and ecosystem productivity.

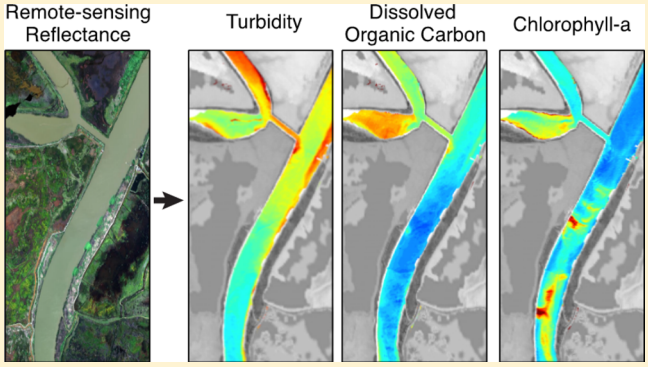

1. INTRODUCTION

The San Francisco Bay–Delta Estuary watershed covers 40% of California, and represents the heart of California's water supply system[1] (Figure 1a). The San Joaquin and Sacramento rivers converge in Central California and form the inverted Sacramento–San Joaquin River Delta (hereafter the Delta). The Delta flows directly into Suisun Bay, and eventually into the greater San Francisco Bay via Carquinez Strait. Half of California's entire streamflow transits through this watershed,[2] and about 9 km^3 of water is exported annually from the Delta to the San Joaquin Valley, the Central Coast of California, and Southern California. Overall, the Delta supplies freshwater to >1 million hectares of agricultural land, and to >27 million people in California via the Central Valley Project (CVP) and State Water Project (SWP) infrastructures.

The San Francisco Bay–Delta Estuary and its watershed is also a very altered and managed ecosystem.[1] Suisun Bay, the adjacent Suisun Marsh, and the Delta (Figure 1a) were once a vibrant and productive tidal marsh consisting of periodically flooded, low-lying islands made of peat and tule, and surrounded by narrow sloughs. But since the mid-19th Century, more than 120 000 ha of tidal marshes have been leveed, drained, and converted to agriculture. About fifty-five levied islands surrounded by deep, barren channels now replace the shallow and dendritic marshlands of the Delta, and a large fraction of the Suisun Marsh is now managed wetlands (Figure 1a). Large water pumping stations in the southern part of the Delta, and upstream regulation of the rivers have also dramatically altered the natural flow of water through the Bay–Delta Estuary. These geomorphological and hydrological alterations have led to the unnatural separation and isolation of terrestrial and aquatic habitats, severe subsidence on the leveed islands, loss of habitat and biodiversity, and the deterioration of water quality.

Water quality monitoring is a key component in the management of this important water resource and ecosystem. Poor water quality can lead to costly drinking-water treatment, and impact ecosystem productivity, habitat quality, and wildlife and human health. The importance of the Delta as a water

Received: July 20, 2015
Revised: December 14, 2015
Accepted: December 14, 2015
Published: December 14, 2015

DOI: 10.1021/acs.est.5b03518
Environ. Sci. Technol. 2016, 50, 573–583

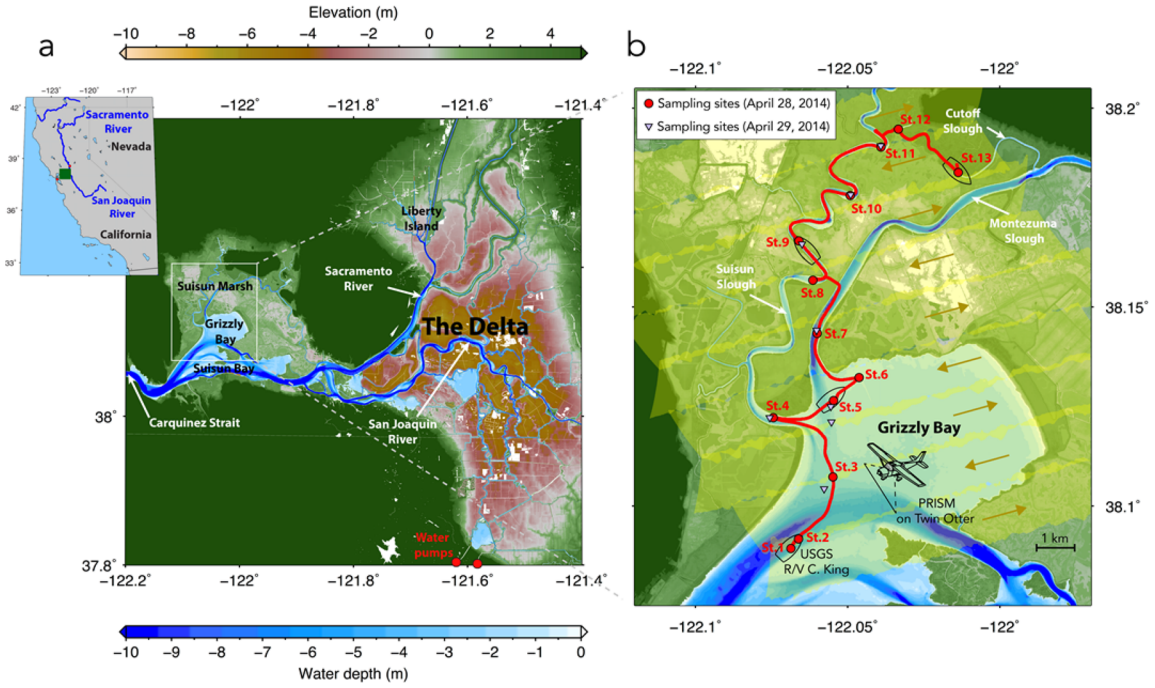

Figure 1. Study site and data collection. (a) Eastern part of San Francisco Bay–Delta Estuary. The Delta is located at the confluence of the Sacramento and San Joaquin rivers and flows into Suisun Bay. The study site is outlined by the white box, and includes a subembayment of Suisun Bay (Grizzly Bay) and the adjacent Suisun Marsh. (b) Simultaneous data collection of airborne remote-sensing reflectance and in situ water quality indicators in Suisun Marsh and Grizzly Bay. Maps were generated with Generic Mapping Tools 5 and a digital elevation model from the Department of Water Resources.

resource, and the deterioration of its ecosystem have recently led to the establishment of a comprehensive, long-term management plan (the Delta Plan) to achieve the coequal goals of "providing a more reliable water supply for California and protecting, restoring, and enhancing the Delta ecosystem".[1] Effective water management and restoration of the ecosystem must be informed by a well-coordinated water quality monitoring effort. The current strategy relies primarily on an array of ∼30 fixed, continuous-monitoring stations (http://ca.water.usgs.gov/projects/baydelta/). While this network of stations provides continuous and long-term background monitoring at selected sites, it lacks the spatial coverage often required to adequately understand the mechanisms driving changes in water quality in this dynamic and heterogeneous environment.

Remote sensing can enhance the water quality monitoring strategies currently used in the San Francisco Bay–Delta Estuary. Important water quality indicators such as turbidity, suspended particles, dissolved organic matter, and chlorophyll-a (chl-a) directly affect the apparent optical properties of the water, and are therefore amenable to remote sensing techniques based on visible and near-infrared imaging spectroscopy.[3,4] Airborne sensors are able to provide better spatial resolution and coverage needed to characterize and understand water-quality dynamics in the optically complex waters of inland water bodies and estuaries.[5−11] Here, hyperspectral imaging from the airborne portable remote imaging spectrometer (PRISM)[12−15] was used to derive multiple water-quality indicators at very high spatial resolution (2.6 × 2.6 m) in the San Francisco Bay–Delta Estuary, and to demonstrate the utility of high-resolution imaging spectroscopy for water quality monitoring and water management in this important water resource and human-impacted ecosystem.

2. EXPERIMENTAL SECTION

Study Site. The area encompassing Grizzly Bay (subembayment of Suisun Bay) and the adjacent Suisun Marsh was chosen as the study site (Figure 1). This area is a salinity transition zone that regularly overlaps with the low-salinity zone (salinity: 0.5–6 psu).[2] It exhibits a wide range of optical properties and water quality, and includes water bodies ranging in size from a 6-km-wide bay to narrow tidal sloughs a few meters wide. Water quality is influenced by natural marsh inputs, as well as a variety of human-derived effluents (e.g., water treatment plants, duck-club ponds). Although sparsely monitored with in situ instrumentation, this region comprises the largest contiguous swath of wetland acreage in the San Francisco Bay–Delta Estuary, including protected historic marshes, managed wetlands and state-targeted areas of future wetland restoration.[16] These characteristics make this study site particularly suitable to demonstrate the utility of high-resolution remote sensing for the large-scale monitoring of water quality.

Data Collection Overview. Airborne radiometric measurements, and in situ measurements of optical properties and water quality indicators were acquired simultaneously over the study area on April 28, 2014 (Figure 1b). Data collection (airborne and in situ) lasted for about 2 h (3:30–5:15 pm PDT) during peak high tide, when water movement was minimal. Atmospheric conditions were clear, except for a few cumulus clouds, wind speeds were <5 m s^{-1}, and the water surface was essentially flat calm. The south-north data collection pattern (Figure 1b) was designed to maximize the range of optical water-quality indicators and minimize any time difference between airborne and in situ measurements. Note the flight lines are oriented as to fly in and out of the sun, in order to minimize sun glint. The data collected on April 28 was used for algorithm development (training data set). A very

DOI: 10.1021/acs.est.5b03518
Environ. Sci. Technol. 2016, 50, 573−583

similar data collection was done on April 29, 2014 (9:15−11:15 am PDT) during low tide. A problem with the positioning system prevented georeferencing and orthorectification of the April 29 airborne data. As a result, only the airborne data collected over a few fixed stations located manually by reference to specific land features were used (Figure 1b). The April 29 data (validation data set) were used to evaluate the algorithms developed using the April 28 training data set. Finally, a third PRISM flyover was done on May 07, 2014 (3:30−5:15 pm PDT) during low tide, but no in situ data were collected.

Underway in Situ Measurements. Field measurements of optical water-quality indicators were collected underway and continuously during the 2 h transect using a custom-made flow-through system installed on the USGS R/V *Mary Lansteiner* (Figure 1b). Three underway measurements of water quality were used in this study. First, turbidity was measured using a Yellow Springs Instruments (YSI) EXO2 water-quality sonde (ISO-7027 method, 860 nm emitter, 90° scattering), and is reported here in Formazin Nephelometric Units (FNU). Second, the fluorescence of chromophoric dissolved organic matter (CDOM) was measured using a customized WETLabs WETStar fluorometer (excitation/emission: 310 nm/452 nm). Third, chlorophyll-a fluorescence was measured using the WETLabs WETStar fluorometer (excitation/emission: 460 nm/695 nm). The performance of the flow-through system and the reliability of the underway water quality measurements made were thoroughly tested.[17,18] The raw CDOM fluorescence was used as an optical proxy for DOC concentration (described later in this manuscript). Raw chl-a fluorescence were converted to units of $\mu g\ L^{-1}$ by using a linear calibration. The calibration was derived from a set of 122 measurements of the chl-a fluorescence paired with chl-a concentrations measured by high precision liquid chromatography on discrete water samples collected in the Suisun Marsh and Grizzly Bay area in 2013. A detailed description of the flow-through system, assessments of its reliability, and chl-a fluorescence calibration are provided in the Supporting Information.

Discrete In Situ Samples and Laboratory Analyses. Discrete water samples were collected at selected stations on April 28−29, 2014 (Figure 1b) for laboratory analyses of dissolved organic carbon (DOC) concentration, chromophoric dissolved organic matter (CDOM) absorption coefficient spectra, filter-passing methylmercury (MeHg) concentration, and total suspended sediment (TSS) concentration. Water for DOC, CDOM, and filter-passing MeHg analysis was pumped directly from the surface (0.5 m deep) using a pump and precleaned, tygon tubing, and was filtered onboard through an inline 0.2 μm GE Memtrex pleated nylon membrane filter. This sampling approach has been thoroughly tested for potential contamination issues and has been used in previous studies.[17,18] Samples for DOC and CDOM were collected in 125 mL amber glass bottles and kept cool (4 °C) until analysis. DOC concentration was measured using high temperature combustion[19,20] (Shimadzu TOC-5000A) within 48 h of collection. CDOM absorbance between 250 and 700 nm was measured using a Cary model 300 spectrophotometer and a 1 cm-path length cuvette, and were converted to Napierian absorption coefficients as in Fichot and Benner (2011).[21] Filter-passing MeHg samples were collected in clean 125 mL Nalgene PETG bottles, acidified with 2.5 mL of 50% hydrochloric acid, and stored at 4 °C until analysis. Filter-passing MeHg was assayed within 5 months of collection by distillation followed by quantification via aqueous-phase ethylation, gas chromatographic separation with cold vapor atomic fluorescence detection on an automated MeHg analyzer (MERX, Brooks Rand Laboratories).[22,23] Samples for TSS concentration were collected unfiltered from the pump in 1 L plastic bottles, and kept cool (4 °C) until analysis. Collecting TSS samples using a pump was appropriate here because the suspended sediment is composed almost entirely of fine sediment.[24] TSS concentration was measured within 48 h of collection and calculated gravimetrically on particles collected after filtration of whole water samples (250 mL) through a 0.45 μm mesh and oven-dried to constant weight.

Note that 11 samples for DOC and CDOM analyses were also collected on April 28, 2014 in the vicinity of Liberty Island (Figure 1b) and were paired with coincident measurements of WETStar CDOM fluorescence from the underway system. These samples were used to develop an optical proxy for DOC concentration (described below).

Development of an Optical Proxy for DOC. Dissolved organic matter (and its carbon content, DOC) consists of a heterogeneous mixture of organic molecules.[25] Only a fraction of it, usually referred to as chromophoric dissolved organic matter or CDOM, absorbs solar radiation in the ultraviolet−visible spectral domain and is directly amenable to imaging spectroscopy.[25] Nevertheless, the CDOM absorption coefficient has been shown to be strongly and linearly correlated with DOC concentration in many riverine, estuarine, and coastal systems, including the San Francisco Bay−Delta Estuary,[17,26−29] where rivers and marshes act as dominant sources of CDOM and DOC. As a result, the CDOM absorption coefficient has often been used as an optical proxy for DOC concentration and an intermediary when estimating DOC concentration from remote sensing in such environments.[27,30,31] Here, a very strong linear relationship (R^2 = 0.985, p < 0.0001) between DOC concentration and the CDOM absorption coefficient at 440 nm, a(440), was also observed for 39 samples collected in the Suisun Marsh and Grizzly Bay area (n = 28) and near Liberty Island (n = 11) (Figure 2a). An analogous relationship (R^2 = 0.985, p < 0.0001) was observed between DOC concentration and the WETStar CDOM fluorescence for those same samples (Figure 2b), and indicated CDOM fluorescence was an excellent proxy for DOC

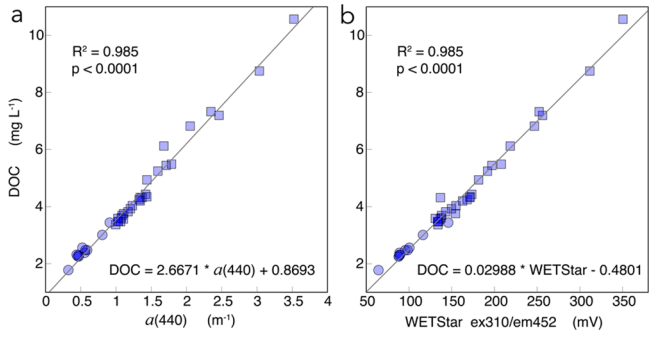

Figure 2. Relationship between dissolved organic carbon (DOC) concentration measured by high-temperature combustion and: (a) the absorption coefficient of CDOM at 440 nm, a(440), and (b) the WETStar CDOM fluorescence (excitation at 310 nm, emission at 452 nm). The relationship is shown for 39 samples collected in the Suisun Marsh and Grizzly Bay area on April 28−29, 2014 (squares, n = 28), and near Liberty Island (see Figure 1b) on April 28, 2015 (circles, n = 11). The relationship between a(440) and the WETStar CDOM is not shown here but was also excellent with a R^2 = 0.979.

DOI: 10.1021/acs.est.5b03518
Environ. Sci. Technol. 2016, 50, 573−583

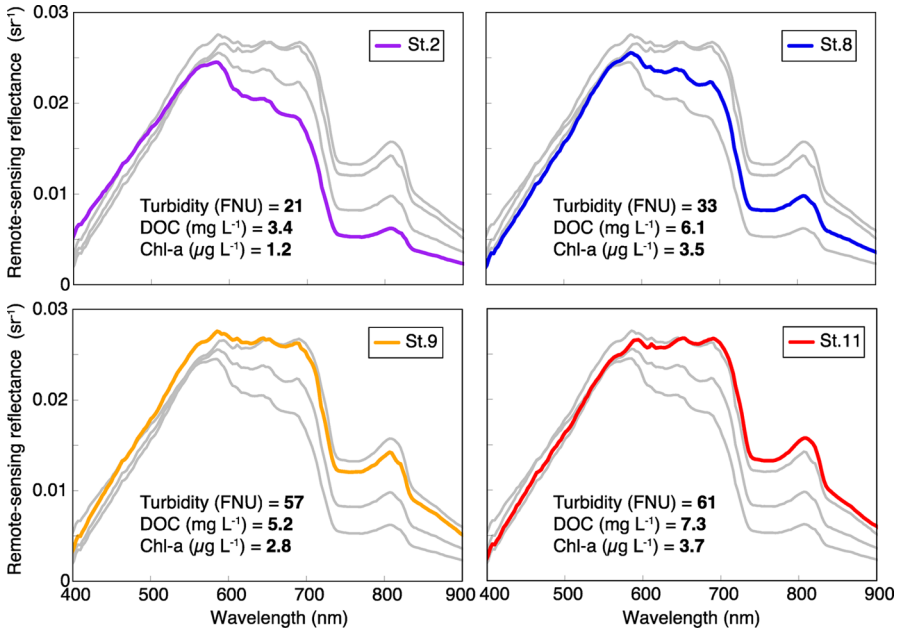

Figure 3. Four contrasting examples of PRISM remote-sensing reflectance spectra selected from the ~7000 spectra paired with coincident in situ water quality measurements acquired underway along the USGS R/V *Mary Lansteiner* track (see Figure 1b). The spectra collected over stations St. 2, St. 8, St. 9, and St. 11 (locations shown in Figure 1b) were selected because they correspond to contrasting water quality conditions.

concentration in this system. The corresponding linear regression (equation in Figure 2b) was used to convert the measured WETStar CDOM fluorescence acquired continuously in situ into a large number (n > 7000) of DOC concentration estimates for use in the development of DOC algorithms (described later in this manuscript).

Airborne Remote-Sensing Reflectances. Remote-sensing reflectance spectra, $R_{rs}(\lambda)$ (λ = 350−1050 nm spectral range, 2.83 nm spectral resolution), were acquired over the study area with the PRISM instrument mounted on a Twin Otter aircraft. PRISM is a push-broom spectrometer (http://prism.jpl.nasa.gov) with high signal-to-noise ratio (500 at 450 nm), low sensitivity to polarization (<1%), and high spectral uniformity (>95%), making it particularly suitable for the remote sensing of coastal and inland waters at very high spatial resolution.[12,13] PRISM was flown at an altitude of 20 000 ft (~6100 m), thereby acquiring radiometric measurements with a 2.6 m spatial sampling. The PRISM raw radiance counts were georeferenced, orthorectified, converted to calibrated radiances using laboratory-determined calibrations, and finally converted to $R_{rs}(\lambda)$ by inverting an atmospheric radiative transfer model. The model uses the ATREM atmospheric correction[32,33] modified by Thompson et al.[34] Additional details about the PRISM data processing are in the Supporting Information.

Algorithms. Three different algorithms for the retrieval of turbidity, DOC, and chl-a were developed using partial-least-squares (PLS) regressions of the hyperspectral $R_{rs}(\lambda)$ data. The PLS-regression models were developed using the April 28 training data set, evaluated using the April 29 validation data set, and implemented on the April 28 and May 07 PRISM data. First, each in situ water quality measurement was matched with the average of 25 $R_{rs}(\lambda)$ spectra acquired over a 5 × 5 pixels area centered on the location of the in situ measurement. A total of about 7000 $R_{rs}(\lambda)$ spectra were paired with corresponding in situ water quality measurements. The paired measurements and the Matlab software (Statistics toolbox and "*plsregress*" function) were then used to perform separate PLS regressions of the fully spectrally resolved PRISM $R_{rs}(\lambda)$ on turbidity, DOC, and chl-a. PLS regression is a well-established multivariate statistical method commonly used in chemometric analysis for constructing predictive models when predictors are numerous and highly collinear. PLS regression is used to reduce complex, fully resolved spectra into a small set of PLS components (linear combinations of the original spectra) that have optimal predictive capability for a given variable of interest.[35,36] Here, the PLS regressions of the fully spectrally resolved PRISM $R_{rs}(\lambda)$ produced new PLS components with optimal predictive capability for the water quality indicators.

A different PLS-regression model was produced and optimized (e.g., optimal wavelength range, and optimal number of PLS components) for each water quality indicator. All models were parametrized using the April 28 training data set, and the April 29 validation data set was used to ensure the PLS-regressions were not overfitted. For turbidity, the best PLS-regression model obtained using this data set used the first 2 PLS components of the fully resolved $R_{rs}(\lambda)$ spectrum in the 529−929 nm spectral range (R_{rs}(529−929) at ~3 nm resolution). For DOC, using the first three PLS components of the fully resolved $R_{rs}(\lambda)$ spectrum in the 478−702 nm spectral range (R_{rs}(478−702) at ~3 nm resolution) produced the best model. Finally, using the first 4 PLS components of the fully resolved $R_{rs}(\lambda)$ spectrum in the 478−787 nm spectral range (R_{rs}(478−787) at ~3 nm resolution) produced the best model to retrieve chl-a. Note here the PLS-regression represents an empirical approach, but it enables effective use of most of the information in the fully resolved $R_{rs}(\lambda)$ spectra. Additional details about the development of the PLS-regression models, information necessary to implement the algorithms (including a spreadsheet to facilitate implementation on individual Rrs(λ) spectra) is provided in the Supporting Information.

DOI: 10.1021/acs.est.5b03518
Environ. Sci. Technol. 2016, 50, 573−583

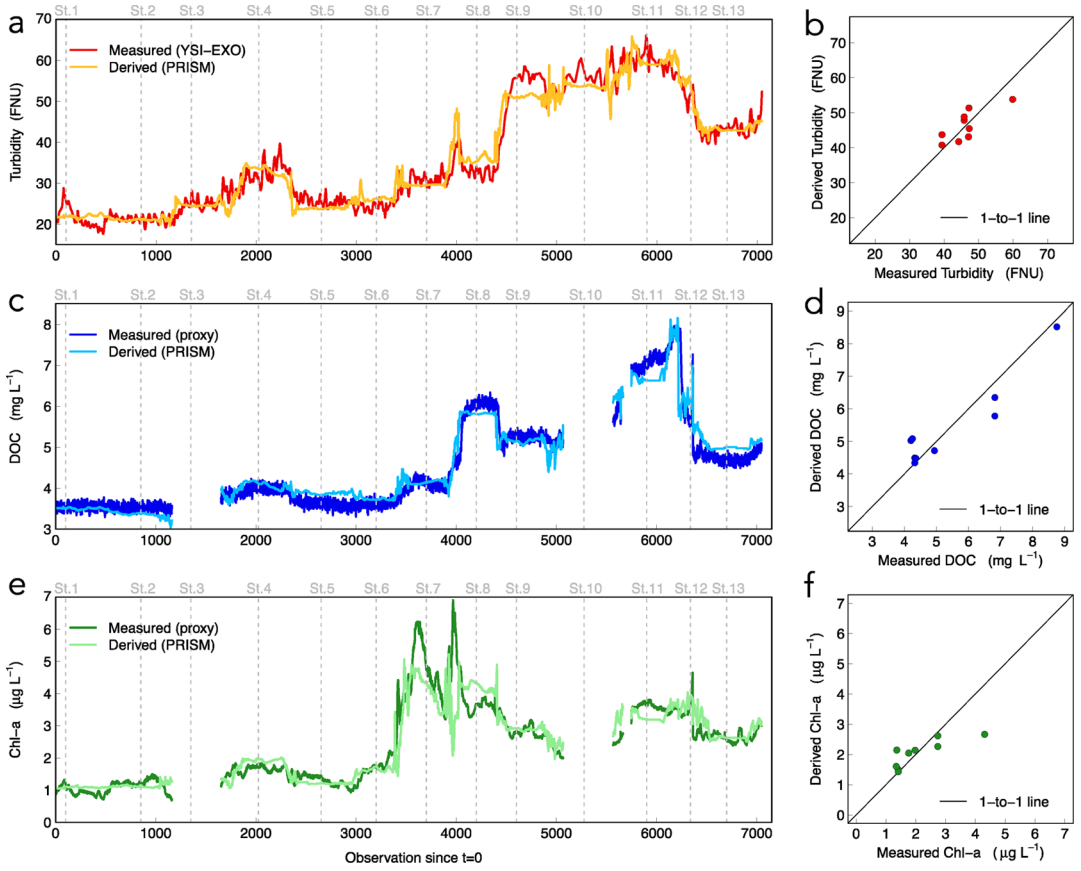

Figure 4. In situ measured and PRISM-derived water quality indicators along the April 28 underway sampling track (see Figure 1b): turbidity (a), DOC (c), and chl-a (e). The location of Stations 1−13 is shown in Figure 1b. The right-panel plots show the validation of the PLS-algorithms using the data collected on April 29 (see Figure 1b): turbidity (b), DOC (d), and chl-a (f).

3. RESULTS AND DISCUSSION

PRISM Remote-Sensing Reflectances. The $R_{rs}(\lambda)$ spectra collected by PRISM over the study area were characteristic of estuarine waters that are optically dominated by suspended sediments, and by dissolved organic matter to a lesser extent[11,37−41] (Figure 3). The $R_{rs}(\lambda)$ spectra exhibited relatively high values at λ > 600 nm, and were very similar in shape and magnitude to spectra collected in other highly turbid estuarine environments.[39,42] The enhanced $R_{rs}(\lambda)$ values result from backscattering by suspended sediments,[39] and the magnitudes of the PRISM $R_{rs}(\lambda)$ values at λ > 600 nm were evidently linked to the turbidity level of the water (Figure 3). Although turbidity also affects $R_{rs}(\lambda)$ values at λ < 600 nm, the effect was confounded by variations in CDOM and DOC. Because the CDOM absorption coefficient spectrum increases exponentially with decreasing wavelength, increased levels of CDOM and DOC typically lead to a preferential decrease in $R_{rs}(\lambda)$ at shorter wavelengths.[37] As a result, high-DOC waters exhibited lower $R_{rs}(\lambda)$ values in the 400−600 nm range (Figure 3). This effect was particularly obvious when comparing the $R_{rs}(\lambda)$ spectra of St. 9 and St. 11, which had comparable turbidities (57 and 61 FNU) but a 40% higher DOC concentration at St. 11. Finally, the effects of variations in phytoplankton biomass on the $R_{rs}(\lambda)$ were subtle and largely confounded by the effects of turbidity and DOC (Figure 3). Phytoplankton biomass and primary production in the San Francisco Bay−Delta Estuary are notoriously low,[43−45] a fact reflected in the generally low chl-a levels measured in this study. Many inland water bodies with lower turbidity and with higher phytoplankton biomass than in this system often exhibit pronounced reflectance peaks near 550 nm and also between 690 and 710 nm.[10,40] Here, a peak between ∼690 to 700 nm was observed but it remained a subdominant feature of the $R_{rs}(\lambda)$ spectra (Figure 3).

In Situ Water Quality Transect. In situ turbidity, DOC, and chl-a all varied several-fold along the south-north track leading from Grizzly Bay to Suisun Marsh, and exhibited distinct variability patterns (Figure 4). Turbidity increased from ∼20 FNU in Grizzly Bay (St. 1, St. 2) to >60 FNU in the upper reaches of Suisun Slough (St. 11), before decreasing progressively with distance to ∼40 FNU at Cutoff Slough (St. 13), which links Suisun Slough to Montezuma Slough (Figure 4a). DOC exhibited the same increasing pattern between Grizzly Bay (3.5−4 mg L^{-1}) and St. 11 in Suisun Slough (∼8 mg L^{-1}), and also decreased to ∼5 mg L^{-1} in Cutoff Slough. However, a distinct pattern of high DOC (>6 mg L^{-1}) and relatively low turbidity (∼30 FNU) was observed near St. 8, and was indicative of a local but substantial source of DOC to this area. Conversely, the portion of Suisun Slough between St. 9 and St. 10 had comparatively low DOC (5 mg L^{-1}) and high turbidity (∼60 FNU). Chl-a concentrations were low, and showed a general increase from the bay (1 µg L^{-1}) to the sloughs of the upper marsh (3 µg L^{-1}). In contrast to DOC and turbidity, maximum chl-a concentrations were observed in the lower reach of Montezuma Slough (near St. 7) and near St. 8. Cross-correlation examination between the three water-quality indicators showed low correlation between chl-a and either turbidity (R^2 = 0.37) or DOC (R^2 = 0.42). Turbidity and DOC were more highly correlated (R^2 = 0.78). These observed

DOI: 10.1021/acs.est.5b03518
Environ. Sci. Technol. 2016, 50, 573−583

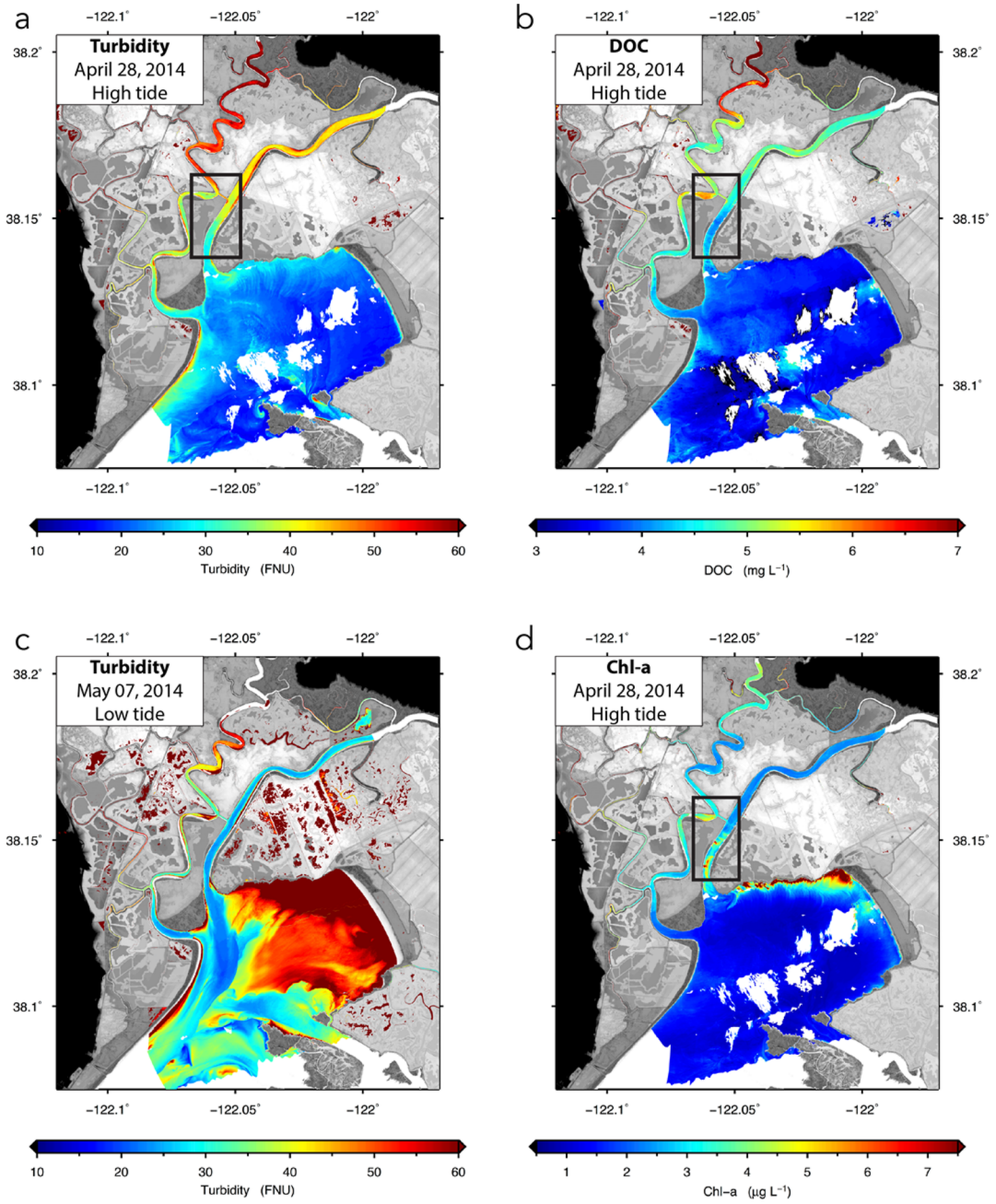

Figure 5. Maps of turbidity, DOC, and chl-a derived by implementing the PLS-based algorithms on PRISM remote-sensing reflectance: (a) Turbidity on April 28, 2014 during high tide, (b) DOC on April 28, 2014 during high tide, (c) Turbidity on May 07, 2014 during low tide, (d) chl-a on May 07, 2014 during high tide. The black box shown in (a), (b), and (d) correspond to the area shown in the abstract figure.

variability patterns reflect the important influence of the tidal marsh on water quality (stations 7−13), but also indicate that distinct processes are regulating each water quality indicator. These patterns are also ideal for evaluating how PRISM is able to reproduce distinct spatial distributions of independent water quality indicators.

Water Quality Algorithms. For the April 28 calibration data set, between 81% and 95% of the observed variance in in situ turbidity, DOC, and chl-a could be reproduced using the PRISM $R_{rs}(\lambda)$ (Figure 4a, c, e). About 95% of the observed variance in in situ turbidity was reconstituted from the PRISM measurements acquired along the April 28 in situ track (Figure 4a), and PRISM-derived estimates of turbidity were on average within ±6% of the turbidity measured in situ. Similarly, about 93% of the observed variance in in situ DOC was reconstituted. The PRISM-derived DOC values were within ±5% of in situ DOC proxy values (Figure 4c), and within ±9% of the DOC concentrations measured by high-temperature combustion when the additional uncertainty of using a DOC proxy was taken into account. About 81% of the in situ chl-a variability was reconstituted using the PRISM data, and retrievals were within ±13% of the measured chl-a proxy values. The algorithm was developed using a chl-a proxy, so a more realistic uncertainty for the retrieval of chl-a concentration was estimated at around ±60%. This uncertainty is relatively large, but does not prevent the detection of phytoplankton blooms that enhance chl-a by several-fold. Nonpigmented particles (inorganic particles, detritus) and CDOM are often

DOI: 10.1021/acs.est.5b03518
Environ. Sci. Technol. 2016, 50, 573−583

dominant drivers of optical variability in highly turbid environments.[46−49] In this specific environment, the elevated concentrations of DOC and inorganic particles, and the relatively low in situ chl-a concentrations contributed to making chl-a optically subdominant and harder to retrieve accurately.

The PLS-regression derived using the April 28 data set produced accurate retrievals of turbidity, DOC, and chl-a when implemented on the April 29 data set (Figure 4b, d, f). The PRISM flyover and coincident in situ data collected on April 29 enabled the evaluation of the algorithms trained using the April 28 data. The retrievals' accuracy on April 29 (turbidity: ±7% ; DOC concentration: ±8%; chl-a proxy: ±18%) was comparable to that of the April 28 retrievals, even though the illumination conditions and tidal stage on April 29 (morning, low tide) were very different from those of April 28 (afternoon, high tide). This consistency using contrasting data sets is evidence that the PLS-regressions were well constrained. More specifically, the number of predictive components used in each PLS-regression was optimal, and the accurate retrievals using the April 29 data demonstrated the models were not overfitted. The algorithms were developed for prevalent dry-season conditions and are expected to perform reasonably well during future implementations in this region of the San Francisco Bay−Delta Estuary. However, the empirical nature of the algorithms imply that further development and validation are needed to make them applicable to other regions of the Bay−Delta Estuary and for periods of high freshwater inflow when optical conditions can be well beyond the range of those encountered in this study.

Remote Sensing of Water Quality at High Spatial Resolution. Implementation of the PLS-regression algorithms on the April 28 and May 07 PRISM data revealed distinct and highly detailed surface distributions of turbidity in Grizzly Bay and Suisun Marsh (Figure 5a, c). Turbidity increased steeply from the bay to the sloughs during high tide on April 28 (Figure 5a). Maximum turbidity levels (>50−60 FNU) were observed in the upper Suisun Slough. This maximum turbidity zone could result from local erosion of the channel, or more likely, from the entrapment of sediment by tidal asymmetries in this isolated dead-end channel.[50] Higher turbidity (>50−60 FNU) was also observed on the inner, shallower edges of the sloughs, consistent with enhanced sediment resuspension in these zones. Variations in turbidity were also observed in Grizzly Bay near land features and over shallows, possibly due to shoreline erosion or wind-wave resuspension in the shallowest waters. The surface distribution of turbidity was very different during low tide on May 07, when maximum turbidity levels (>50−60 FNU) were observed in Grizzly Bay (Figure 5c). This observation is consistent with previous observations that suspended sediment concentrations are highest in Grizzly Bay during low tide.[51] Low tide probably enhanced sediment resuspension in the shallow Grizzly Bay because wind waves attenuate rapidly with water depth and resuspension is more likely in shallow waters. Ebb tide on May 07 was also flowing in opposite direction to a westerly wind of 2−3 m s^{-1} (NOAA station 9415144), and could have produced steeper waves that further enhanced resuspension. The diffuse attenuation of solar radiation in these waters is high enough that the influence of bottom reflectance on remote-sensing reflectance is insignificant, even in the very shallow parts of Grizzly Bay. Minimum turbidity (20−30 FNU) was observed in Montezuma Slough, which connects Grizzly Bay to an upstream and major channel of the Delta located at the confluence of the Sacramento and San Joaquin Rivers. The contrast between April 28 and May 07 illustrates the extreme heterogeneity and dynamic nature of turbidity in this region, and highlights the complexity of the processes driving its variability.

The spatial distributions of DOC and chl-a retrieved with PRISM on April 28 were distinct from that of turbidity, and exhibited unique features (Figure 5a, b, d). DOC concentrations were relatively homogeneous in Grizzly Bay and increased progressively in the narrowing sloughs to reach a maximum in the upper Suisun Slough, consistent with the marsh acting as an important source of organic matter. The high-DOC, low-turbidity feature revealed by the in situ data (near St. 8) was clearly identified in the scenes as a surface pool of high-DOC water originating from a small channel west of the pool (Figure 5a, b). Chl-a concentrations were low (<2 μg L^{-1}) and varied very little in most of Grizzly Bay, in agreement with previous findings.[52] However, the PRISM data revealed higher chl-a concentrations (>7 μg L^{-1}) on the northeastern shore of Grizzly Bay (Figure 5d). Higher levels of chl-a were also observed in the lower part of Montezuma Slough, in agreement with the chl-a maximum (6−7 μg L^{-1}) observed with the in situ data near St. 7. Higher levels of chl-a (4−5 μg L^{-1}) were also found in the upper Suisun Slough, consistent with the marsh supplying nutrients, and a longer residence time of the water in these channels. Effluent from the Fairfield-Suisun Sewer District wastewater treatment plant (67 million L of wastewater treated every day) is potentially a significant source of nutrients and DOC to the upper Suisun Slough (discharge point is in Boynton Slough which connects directly to Suisun Slough). The distinct spatial distributions of turbidity, DOC, and chl-a derived with PRISM demonstrate how a single hyperspectral image can provide valuable insights to untangle the complexity of water quality metrics in temporally dynamic coastal and inland waters.

Remotely sensed turbidity can be used to infer the distribution of suspended particles and provide valuable quantitative information for our understanding of sediment transport in estuaries. Fundamental questions remain with regard to the sources, sinks, and transport of sediment in the San Francisco Bay−Delta Estuary and in other estuaries, and are partly hindered by a paucity of data on the spatial variability of TSS concentration.[53] Previous work has successfully used remote sensing to derive TSS concentration with reasonable accuracy in the San Francisco Bay−Delta Estuary.[54,55] In this study, in situ turbidity exhibited a strong linear relationship (R^2 = 0.92, p < 0.0001) with measured TSS concentration (Figure 6) and can facilitate the retrieval of TSS concentration from remotely sensed turbidity. A remarkably similar relationship was previously observed in this system.[56,57] The connection between TSS and turbidity is particularly strong in the San Francisco Bay−Delta Estuary because suspended particles are predominantly fine and scatter light efficiently, and particle floc size tends to be spatially homogeneous.[56,57]

The remotely sensed DOC can inform on the distribution, source, and transport of important contaminants like methylmercury in aquatic systems influenced by wetlands. MeHg binds strongly to sulfur-rich groups within dissolved organic matter.[58] As a result, strong relationships between filter-passing MeHg (FMeHg) and either DOC concentration or CDOM optical properties have been observed in some aquatic environments, including some marsh-influenced areas of the San Francisco Bay−Delta Estuary.[18,59−62] Wetland sediments

DOI: 10.1021/acs.est.5b03518
Environ. Sci. Technol. 2016, 50, 573−583

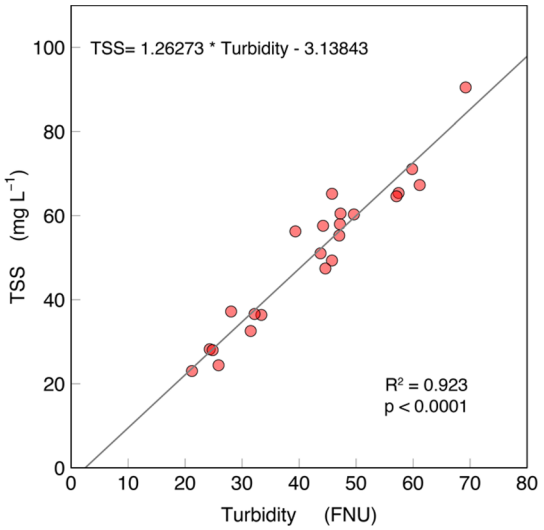

Figure 6. Total suspended sediment (TSS) concentration versus turbidity for samples collected in the Suisun Marsh and Grizzly Bay area on April 28–29, 2014. Sample locations are shown in Figure 1b.

are important sites of MeHg production by sulfate-reducing and iron-reducing bacteria,[63−65] and tidal transport can effectively export organic-bound MeHg from wetlands to surrounding waters.[18,59,63] The analysis of 28 samples collected on April 28 (high tide) and April 29 (low tide) of 2014 in the study area revealed a significant relationship (R^2 = 0.84, p < 0.0001) between DOC and FMeHg, thereby indicating the spatial distribution of FMeHg in surface water can be derived within reasonable uncertainty from the remotely sensed DOC (Figure 7). FMeHg concentrations were elevated in the primary slough channels relative to the open water of Grizzly Bay, and increased progressively to reach maximum concentrations in the upper Suisun Slough and near the marsh. This simple approach can help identify potential hot spots of contaminants in wetland-influenced water bodies. However, the relationship between DOC and FMeHg is likely to vary over time or between regions of the San Francisco Bay–Delta Estuary, because the organic-contaminant interactions can be affected by a variety of factors such as the sources and sinks of MeHg, or the chemical composition of dissolved organic matter. Our ability to remotely sense the concentration of organic-bound contaminants like MeHg therefore hinges on the reliability of their relationships with DOC within a given system.

Application for Resource Management. A number of studies have successfully demonstrated the possibility of deriving spatial distribution of water quality indicators using airborne hyperspectral imagery in rivers, lakes and estuarine environments.[5−11] Here, PRISM successfully facilitated the simultaneous retrieval of multiple water quality indicators at high spatial resolution in the optically complex waters of the San Francisco Bay–Delta Estuary. The simultaneous retrieval of multiple water quality indicators at high spatial resolution from a single hyperspectral image can facilitate the detection of point-source pollution and help assess the impacts of ecosystem restoration and climate-driven changes on water quality. High-resolution imagery of independent water quality indicators can provide a means to directly detect and discriminate between different types of effluents, and facilitate identification of their source in coastal and inland waters. High-resolution remote sensing can also help monitor and understand the more diffuse and complex effects of wetland restoration on water quality. Wetlands are an important source of DOC and MeHg to downstream waters.[18,59] DOC is a precursor for undesired water disinfection byproducts,[66,67] and MeHg is a potent neurotoxin of particular concern in the Bay–Delta Estuary[68,69] and in many inland and coastal systems globally. Wetland restoration projects, like those defined in the Delta Plan,[1] can potentially lead to higher levels of DOC and MeHg in surrounding waters. The routine use of high-resolution imagery could facilitate the monitoring of water quality on spatial scales that are adequate to assess these potential impacts of wetland restoration. It could also facilitate the assessment of the short and long-term effects of changes in precipitation, freshwater

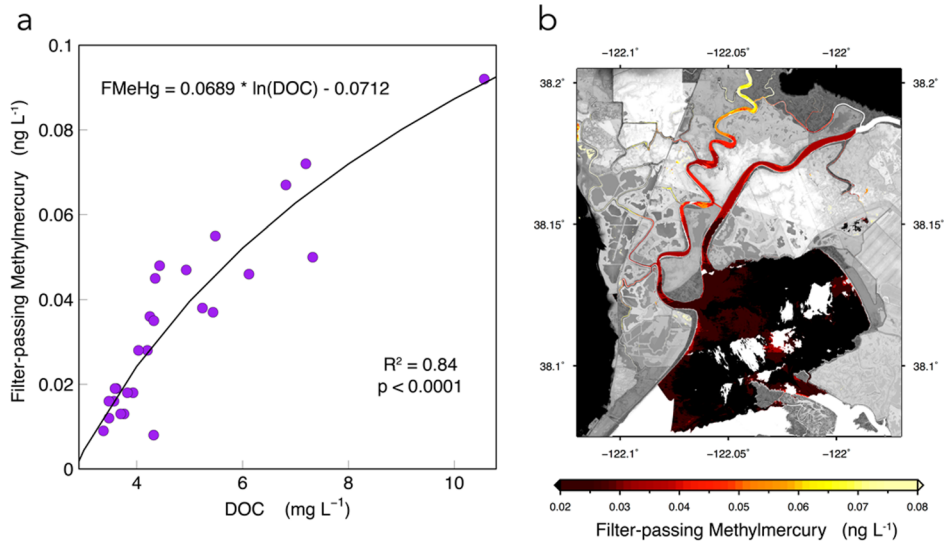

Figure 7. (a) Filter-passing methylmercury concentrations versus dissolved organic carbon (DOC) concentrations for samples collected in the Suisun Marsh and Grizzly Bay area on April 28–29, 2014. Sample locations are shown in Figure 1b. (b) Distribution of filter-passing methylmercury on April 28, 2014 obtained by applying the FMeHg-DOC relationship shown on panel (a) on the DOC distribution derived from PRISM (see DOC map on Figure 5b).

DOI: 10.1021/acs.est.5b03518
Environ. Sci. Technol. 2016, 50, 573−583

flow, tidal forcing, wind patterns, and other climatic forcing on water quality and water resource reliability.

By enabling the detection of phytoplankton blooms, high-resolution remote sensing can foster a better understanding of the factors regulating biological productivity in inland waters. For instance, the San Francisco Bay−Delta Estuary has exceptionally low primary productivity relative to other estuaries worldwide,[44] with chl-a concentrations of <5 $\mu g\ L^{-1}$ generally observed in Suisun and Grizzly Bays.[43,45,70] The abundance of pelagic fish species in the San Francisco Bay−Delta Estuary has also declined to extremely low levels in the past decade,[71] and is in part associated with the recent decline in phytoplankton abundance also observed in this region.[43] Light limitation, grazing, particle residence time, elevated ammonium concentrations from wastewater effluents, and extensive particle filtering by the invasive clam *Corbula amurensis* are all thought to contribute to the low productivity of the San Francisco Bay−Delta Estuary.[45,70,72−74] Yet, the variables controlling phytoplankton biomass and production in the San Francisco Bay−Delta Estuary have strong temporal and spatial variability.[45,52] Our understanding of phytoplankton dynamics and controlling factors in heterogeneous and dynamic systems like the San Francisco Bay−Delta Estuary could therefore benefit from high-resolution imagery of phytoplankton biomass, as well as from high-resolution imagery of DOC and turbidity which can limit light availability and phytoplankton growth. Furthermore, PRISM-like hyperspectral reflectance has been used to discriminate between phytoplankton functional types in inland and coastal waters, and could facilitate the early detection of harmful algal blooms in our natural water supplies.[75−78]

Water management practices can benefit from detailed, remotely sensed maps of water quality. The Delta smelt is an endangered fish and represents an excellent example of how remote sensing can inform water management decision-making. The protection of the Delta smelt can often limit water-pumping operations in the southern part of the Delta. Delta smelts are often associated with turbidity levels higher than 10−12 NTU,[79,80] and state water agencies typically rely on turbidity monitoring stations to prevent the entrainment of smelts and manage water-pumping operations. However, the spatial coverage is often insufficient to adequately understand and predict variations in turbidity zones in this dynamic and heterogeneous environment. High-resolution imagery can help assess the spatial distribution of specific turbidity features and provide useful insights on how geomorphological and physical processes drive turbidity dynamics (e.g., wind events, drought, and flood events) and affect the spatial distribution of the Delta smelt, as well as of that other threatened fish species (e.g., longfin smelt).

■ ASSOCIATED CONTENT

Supporting Information

. The Supporting Information is available free of charge on the ACS Publications website at DOI: 10.1021/acs.est.5b03518.

Figures S1−S5 (PDF)

MS-Excel spreadsheet for algorithm implementation on individual remote-sensing reflectance spectra (XLS)

■ AUTHOR INFORMATION

Corresponding Author

*Phone: 818-354-5666; fax: 818-354-0966; e-mail: cgfichot@gmail.com.

Notes

The authors declare no competing financial interest.

■ ACKNOWLEDGMENTS

This work was performed at the Jet Propulsion Laboratory, California Institute of Technology, under contract with the National Aeronautics and Space Administration. We thank Scott Nagel for captaining the USGS R/V *Mary Landsteiner*, and Katy O'Donnell, Ryan Carlo, Le H. Kieu, and Adam McClure for helping with logistics and sampling, and Travis VonDessoneck for work on developing the underway flow-through sampling system. We also thank Evangelos Kakouros for methylmercury sample analysis, and Michael Gunson, Ernesto Diaz, Ian Mccubbin, William Mateer, Christopher White, Pantazis Mouroulis, and Byron VanGorp for facilitating the airborne data acquisition. Finally, we thank Matt Ferner for processing the TSS samples, and David Shoellhamer and two anonymous reviewers for their useful comments on the manuscript.

■ REFERENCES

(1) *The Delta Plan 2013. Ensuring a reliable water supply for California, a healthy Delta ecosystem, and a place of enduring value*; Delta Stewardship Council, 2013.

(2) Healey, M. C.; Dettinger, M. D.; Norgaard, R. B. *The State of Bay-Delta Science*, 2008; 2008.

(3) *Remote Sensing of Ocean Colour in Coastal, and Other Optically-Complex, Waters*; Sathyendranath, S., Ed.; Reports of the International Ocean Colour Coordinating Group; IOCCG: Dartmouth, Canada, 2000; Vol. 3.

(4) *Mission Requirements for Future Ocean-Colour Sensors*; McClain, C. R., Meister, G., Eds.; Reports of the International Ocean Colour Coordinating Group; IOCCG: Dartmouth, Canada, 2012; Vol. 13.

(5) Koponen, S.; Pulliainen, J.; Kallio, K.; Hallikainen, M. Lake water quality classification with airborne hyperspectral spectrometer and simulated MERIS data. *Remote Sens. Environ.* **2002**, *79* (1), 51−59.

(6) Thiemann, S.; Kaufmann, H. Lake water quality monitoring using hyperspectral airborne data - A semiempirical multisensor and multitemporal approach for the Mecklenburg Lake District, Germany. *Remote Sens. Environ.* **2002**, *81* (2−3), 228−237.

(7) Sugumaran, R. Monitoring intra-annual water quality variations using airborne hyperspectral remote sensing data in Iowa lakes. *J. Appl. Remote Sens* **2007**, *1* (1), 013533.

(8) Hunter, P. D.; Tyler, A. N.; Carvalho, L.; Codd, G. A.; Maberly, S. C. Hyperspectral remote sensing of cyanobacterial pigments as indicators for cell populations and toxins in eutrophic lakes. *Remote Sens. Environ.* **2010**, *114* (11), 2705−2718.

(9) Moses, W. J.; Gitelson, A. A.; Perk, R. L.; Gurlin, D.; Rundquist, D. C.; Leavitt, B. C.; Barrow, T. M.; Brakhage, P. Estimation of chlorophyll-a concentration in turbid productive waters using airborne hyperspectral data. *Water Res.* **2012**, *46* (4), 993−1004.

(10) Olmanson, L. G.; Brezonik, P. L.; Bauer, M. E. Airborne hyperspectral remote sensing to assess spatial distribution of water quality characteristics in large rivers: The Mississippi River and its tributaries in Minnesota. *Remote Sens. Environ.* **2013**, *130*, 254−265.

(11) Fan, C. *Spectral Analysis of Water Reflectance for Hyperspectral Remote Sensing of Water Quailty in Estuarine Water*, April 19−27, 2014.

(12) Mouroulis, P.; Green, R. O.; Wilson, D. W. Optical design of a coastal ocean imaging spectrometer. *Opt. Express* **2008**, *16* (12), 9087−9096.

(13) Mouroulis, P.; Van Gorp, B.; Green, R. O.; Dierssen, H.; Wilson, D. W.; Eastwood, M.; Boardman, J.; Gao, B.-C.; Cohen, D.;

Franklin, B.; et al. Portable Remote Imaging Spectrometer coastal ocean sensor: design, characteristics, and first flight results. *Appl. Opt.* **2014**, *53* (7), 1363−1380.
(14) Dierssen, H. M.; Chlus, A.; Russell, B. Hyperspectral discrimination of floating mats of seagrass wrack and the macroalgae Sargassum in coastal waters of Greater Florida Bay using airborne remote sensing. *Remote Sens. Environ.* **2015**, *167*, 247−258.
(15) Thompson, D. R.; Seidel, F. C.; Gao, B. C.; Gierach, M. M.; Green, R. O.; Kudela, R. M.; Mouroulis, P. Optimizing Irradiance Estimates for Coastal and Inland Water Imaging Spectroscopy. *Geophys. Res. Lett.* **2015**, *42* (10), 4116−4123.
(16) *Suisun Marsh: Ecological History and Possible Futures*; Moyle, P. B., Manfree, A. D., Fiedler, P. L., Eds.; UC Press: Berkeley, CA, 2014.
(17) Downing, B. D.; Boss, E.; Bergamaschi, B. A.; Fleck, J. A.; Lionberger, M. A.; Ganju, N. K.; Schoellhamer, D. H.; Fujii, R. Quantifying fluxes and characterizing compositional changes of dissolved organic matter in aquatic systems in situ using combined acoustic and optical measurements. *Limnol. Oceanogr.: Methods* **2009**, *7*, 119−131.
(18) Bergamaschi, B. A.; Fleck, J. A.; Downing, B. D.; Boss, E.; Pellerin, B.; Ganju, N. K.; Schoellhamer, D. H.; Byington, A. A.; Heim, W. A.; Stephenson, M.; et al. Methyl mercury dynamics in a tidal wetland quantified using in situ optical measurements. *Limnol. Oceanogr.* **2011**, *56* (4), 1355−1371.
(19) Benner, R.; Strom, M. A critical evaluation of the analytical blank associated with DOC measurements by high-temperature catalytic oxidation. *Mar. Chem.* **1993**, *41*, 153−160.
(20) Bird, S. M.; Fram, M. S.; Crepeau, K. L. *Method of Analysis by the U.S. Geological Survey California District Sacramento Laboratory—Determination of Dissolved Organic Carbon in Water by High Temperature Catalytic Oxidation, Method Validation, and Quality-Control Practices*, 2003.
(21) Fichot, C. G.; Benner, R. A novel method to estimate DOC concentrations from CDOM absorption coefficients in coastal waters. *Geophys. Res. Lett.* **2011**, *38* (3), L03610.
(22) De Wild, J. F.; Olsen, M. L.; Olund, S. D. *Determination of Methyl Mercury by Aqueous Phase Ethylation, Followed by Gas Chromatographic Separation with Cold Vapor Atomic Fluorescence Detection*, Version 1, 2002.
(23) Marvin-DiPasquale, M.; Agee, J. L.; Kakouros, E.; Kieu, L. H.; Fleck, J. A.; Alpers, C. N. *The Effects of Sediment and Mercury Mobilization in the South Yuba River and Humbug Creek Confluence Area, Nevada County, California: Concentrations, Speciation and Environmental Fate-Part 2: Laboratory Experiments*, 2011.
(24) Manning, A. J.; Schoellhamer, D. H. Factors controlling floc settling velocity along a longitudinal estuarine transect. *Mar. Geol.* **2013**, *345*, 266−280.
(25) *Biogeochemistry of Marine Dissolved Organic Matter*, 2nd, ed.; Hansell, D. A., Carlson, C. A., Eds.; Academic Press: Boston, 2015.
(26) Del Vecchio, R.; Blough, N. V. Spatial and seasonal distribution of chromophoric dissolved organic matter and dissolved organic carbon in the Middle Atlantic Bight. *Mar. Chem.* **2004**, *89* (1−4), 169−187.
(27) Mannino, A.; Russ, M. E.; Hooker, S. B. Algorithm development and validation for satellite-derived distributions of DOC and CDOM in the U.S. Middle Atlantic Bight. *J. Geophys. Res.* **2008**, *113* (C7), C07051.
(28) Spencer, R. G. M.; Butler, K. D.; Aiken, G. R. Dissolved organic carbon and chromophoric dissolved organic matter properties of rivers in the USA. *J. Geophys. Res.* **2012**, *117* (3), G03001.
(29) Matsuoka, A.; Bricaud, A.; Benner, R.; Para, J.; Sempéré, R.; Prieur, L.; Bélanger, S.; Babin, M. Tracing the transport of colored dissolved organic matter in water masses of the Southern Beaufort Sea: relationship with hydrographic characteristics. *Biogeosciences* **2012**, *9* (3), 925−940.
(30) Matsuoka, A.; Hooker, S. B.; Bricaud, A.; Gentili, B.; Babin, M. Estimating absorption coefficients of colored dissolved organic matter (CDOM) using a semi-analytical algorithm for southern Beaufort Sea waters: application to deriving concentrations of dissolved organic carbon from space. *Biogeosciences* **2013**, *10* (2), 917−927.
(31) Fichot, C. G.; Lohrenz, S. E.; Benner, R. Pulsed, cross-shelf export of terrigenous dissolved organic carbon to the Gulf of Mexico. *J. Geophys. Res. Ocean* **2014**, *119* (2), 1176−1194.
(32) Gao, B.-C.; Heidebrecht, K. B.; Goetz, A. F. H. Derivation of scaled surface reflectances from AVIRIS data. *Remote Sens. Environ.* **1993**, *44* (2−3), 165−178.
(33) Gao, B.-C.; Goetz, F. H. Column Atmospheric Water Vapor and Vegetation Liquid Water Retrievals From Airborne Imaging Spectrometer Data is that the retrieved column water vapor amounts over land /. *J. Geophys. Res.* **1990**, *95* (D4), 3549−3564.
(34) Thompson, D. R.; Gao, B.-C.; Green, R. O.; Roberts, D. A.; Dennison, P. E.; Lundeen, S. R. Atmospheric correction for global mapping spectroscopy: ATREM advances for the HyspIRI preparatory campaign. *Remote Sens. Environ.* **2015**, *167*, 64−77.
(35) Geladi, P.; Kowalski, B. R. Partial least-squares regression: a tutorial. *Anal. Chim. Acta* **1986**, *185*, 1−17.
(36) *Handbook of Partial Least Squares: Concepts, Methods, and Applications*; Esposito Vinzi, V., Chin, W. W., Henseler, J., Wang, H., Eds.; Springer-Verlag Berlin Heidelberg: Berlin, Germany, 2010.
(37) Lee, Z.; Carder, K. L.; Hawes, S. K.; Steward, R. G.; Peacock, T. G.; Davis, C. O. Model for the interpretation of hyperspectral remote-sensing reflectance. *Appl. Opt.* **1994**, *33* (24), 5721−5732.
(38) Doxaran, D.; Froidefond, J.-M.; Castaing, P. Remote-sensing reflectance of turbid sediment-dominated waters. Reduction of sediment type variations and changing illumination conditions effects by use of reflectance ratios. *Appl. Opt.* **2003**, *42* (15), 2623−2634.
(39) Doxaran, D.; Cherukuru, N.; Lavender, S. J. Apparent and inherent optical properties of turbid estuarine waters: measurements, empirical quantification relationships, and modeling. *Appl. Opt.* **2006**, *45* (10), 2310−2324.
(40) Dall'Olmo, G.; Gitelson, A. A. Effect of bio-optical parameter variability and uncertainties in reflectance measurements on the remote estimation of chlorophyll-a concentration in turbid productive waters: modeling results. *Appl. Opt.* **2006**, *45* (15), 3577−3592.
(41) Knaeps, E.; Ruddick, K. G.; Doxaran, D.; Dogliotti, A. I.; Nechad, B.; Raymaekers, D.; Sterckx, S. A SWIR based algorithm to retrieve total suspended matter in extremely turbid waters. *Remote Sens. Environ.* **2015**, *168*, 66−79.
(42) Dogliotti, A. I.; Ruddick, K. G.; Nechad, B.; Doxaran, D.; Knaeps, E. A single algorithm to retrieve turbidity from remotely-sensed data in all coastal and estuarine waters. *Remote Sens. Environ.* **2015**, *156*, 157−168.
(43) Jassby, A. D. Phytoplankton in the upper San Francisco Estuary: Recent biomass trends, their causes and their trophic significance. *San Fr. Estuary Watershed Sci.* **2008**, *6* (1), 1−24.
(44) Cloern, J. E.; Foster, S. Q.; Kleckner, A. E. Phytoplankton primary production in the world's estuarine-coastal ecosystems. *Biogeosciences* **2014**, *11* (9), 2477−2501.
(45) Glibert, P. M.; Dugdale, R. C.; Wilkerson, F.; Parker, A. E.; Alexander, J.; Antell, E.; Blaser, S.; Johnson, A.; Lee, J.; Lee, T.; et al. Major - but rare - spring blooms in 2014 in San Francisco Bay Delta, California, a result of the long-term drought, increased residence time, and altered nutrient loads and forms. *J. Exp. Mar. Biol. Ecol.* **2014**, *460*, 8−18.
(46) Gallegos, C. L.; Neale, P. J. Partitioning spectral absorption in case 2 waters: discrimination of dissolved and particulate components. *Appl. Opt.* **2002**, *41* (21), 4220−4233.
(47) Dall'Olmo, G.; Gitelson, A. A.; Runquist, D. C. Towards a unified approach for remote estimation of chlorophyll-a in both terrestrial vegetation and turbid productive waters. *Geophys. Res. Lett.* **2003**, *30* (18), 1938.
(48) Darecki, M.; Weeks, A.; Sagan, S.; Kowalczuk, P.; Kaczmarek, S. Optical characteristics of two contrasting Case 2 waters and their influence on remote sensing algorithms. *Cont. Shelf Res.* **2003**, *23* (3−4), 237−250.

DOI: 10.1021/acs.est.5b03518
Environ. Sci. Technol. 2016, 50, 573−583

(49) Mobley D, C.; Stramski, D.; Bissett, W. P.; Boss, E. Optical modeling of ocean waters: Is the Case 1 - Case 2 classification still useful? *Oceanography* **2004**, *17* (2), 60−67.
(50) Morgan-King, T. L.; Schoellhamer, D. H. Suspended-Sediment Flux and Retention in a Backwater Tidal Slough Complex near the Landward Boundary of an Estuary. *Estuaries Coasts* **2013**, *36* (2), 300−318.
(51) Warner, J. C.; Schoellhamer, D. H.; Ruhl, C. A.; Burau, J. R. Floodtide pulses after low tides in shallow subembayments adjacent to deep channels. *Estuarine, Coastal Shelf Sci.* **2004**, *60* (2), 213−228.
(52) Kimmerer, W. J.; Parker, A. E.; Lidström, U. E.; Carpenter, E. J. Short-Term and Interannual Variability in Primary Production in the Low-Salinity Zone of the San Francisco Estuary. *Estuaries Coasts* **2012**, *35* (4), 913−929.
(53) Barnard, P. L.; Schoellhamer, D. H.; Jaffe, B. E.; McKee, L. J. Sediment transport in the San Francisco Bay Coastal System: An overview. *Mar. Geol.* **2013**, *345*, 3−17.
(54) Leeuw, T.; Boss, E.; Byrd, K.; Hill, P.; Downing, B.; Fichot, C. Remote sensing of TSM from the ground up: A synthesis of ground, aircraft, and satellite reflectance data. In *Proceedings of the Ocean Optics Conference XXII*; Portland, ME, 2014.
(55) Ruhl, C.; Schoellhamer, D.; Stumpf, R.; Lindsay, C. Combined use of remote sensing and continuous monitoring to analyse the variability of suspended-sediment concentrations in San Francisco Bay, California. *Estuarine, Coastal Shelf Sci.* **2001**, *53*, 801−812.
(56) Ganju, N. K.; Schoellhamer, D. H.; Murrell, M. C.; Gartner, J. W.; Wright, S. A. Constancy of the relation between floc size and density in San Francisco Bay. *Proc. Mar. Sci.* **2007**, *8*, 75−91.
(57) Schoellhamer, D. H.; Wright, S. A.; Drexler, J. Z. Conceptual Model of Sedimentation in the Sacramento − San Joaquin River Delta. *San Fr. Estuary Watershed Sci.* **2012**, *10* (3), 1−25.
(58) Ravichandran, M. Interactions between mercury and dissolved organic matter–a review. *Chemosphere* **2004**, *55* (3), 319−331.
(59) Bergamaschi, B. A.; Krabbenhoft, D. P.; Aiken, G. R.; Patino, E.; Rumbold, D. G.; Orem, W. H. Tidally driven export of dissolved organic carbon, total mercury, and methylmercury from a mangrove-dominated estuary. *Environ. Sci. Technol.* **2012**, *46* (3), 1371−1378.
(60) Tsui, M. T. K.; Finlay, J. C. Influence of dissolved organic carbon on methylmercury bioavailability across minnesota stream ecosystems. *Environ. Sci. Technol.* **2011**, *45* (14), 5981−5987.
(61) Berndt, M. E.; Bavin, T. K. Methylmercury and dissolved organic carbon relationships in a wetland-rich watershed impacted by elevated sulfate from mining. *Environ. Pollut.* **2012**, *161*, 321−327.
(62) Driscoll, C. T.; Blette, V.; Yan, C.; Schofield, C. L.; Munson, R.; Holsapple, J. The role of dissolved organic carbon in the chemistry and bioavailability of mercury in remote Adirondack lakes. *Water, Air, Soil Pollut.* **1995**, *80* (1−4), 499−508.
(63) Hall, B. D.; Aiken, G. R.; Krabbenhoft, D. P.; Marvin-DiPasquale, M.; Swarzenski, C. M. Wetlands as principal zones of methylmercury production in southern Louisiana and the Gulf of Mexico region. *Environ. Pollut.* **2008**, *154* (1), 124−134.
(64) Marvin-DiPasquale, M.; Windham-Myers, L.; Agee, J. L.; Kakouros, E.; Kieu, L. H.; Fleck, J. a.; Alpers, C. N.; Stricker, C. A. Methylmercury production in sediment from agricultural and non-agricultural wetlands in the Yolo Bypass, California, USA. *Sci. Total Environ.* **2014**, *484* (1), 288−299.
(65) Alpers, C. N.; Fleck, J. A.; Marvin-DiPasquale, M.; Stricker, C. a.; Stephenson, M.; Taylor, H. E. Mercury cycling in agricultural and managed wetlands, Yolo Bypass, California: Spatial and seasonal variations in water quality. *Sci. Total Environ.* **2014**, *484* (1), 276−287.
(66) Chow, A. T.; Dahlgren, R. A.; Harrison, J. A. Watershed sources of disinfection byproduct precursors in the Sacramento and San Joaquin Rivers, California. *Environ. Sci. Technol.* **2007**, *41* (22), 7645−7652.
(67) Kraus, T. E. C.; Bergamaschi, B. A.; Hernes, P. J.; Spencer, R. G. M.; Stepanauskas, R.; Kendall, C.; Losee, R. F.; Fujii, R. Assessing the contribution of wetlands and subsided islands to dissolved organic matter and disinfection byproduct precursors in the Sacramento-San Joaquin River Delta: A geochemical approach. *Org. Geochem.* **2008**, *39* (9), 1302−1318.
(68) San Francisco Bay,Regional Water Quality Control Board. *Mercury in San Francisco Bay. Total Maximum Daily Load (TMDL) Proposed Basin Plan Amendment and Staff Report for Revised Total Maximum Daily Load (TMDL) and Proposed Mercury Water Quality Objectives*; Oakland, CA, 2006.
(69) Davis, J. A.; Looker, R. E.; Yee, D.; Marvin-Di Pasquale, M.; Grenier, J. L.; Austin, C. M.; McKee, L. J.; Greenfield, B. K.; Brodberg, R.; Blum, J. D. Reducing methylmercury accumulation in the food webs of San Francisco Bay and its local watersheds. *Environ. Res.* **2012**, *119*, 3−26.
(70) Wilkerson, F. P.; Dugdale, R. C.; Hogue, V. E.; Marchi, A. Phytoplankton Blooms and Nitrogen Productivity in San Francisco Bay. *Estuaries Coasts* **2006**, *29* (3), 401−416.
(71) Sommer, T.; Armor, C.; Baxter, R.; Breuer, R.; Brown, L.; Chotkowski, M.; Culberson, S.; Feyrer, F.; Gingras, M.; Herbold, B.; et al. The Collapse of Pelagic Fishes in the Upper San Francisco Estuary: El Colapso de los Peces Pelagicos en La Cabecera Del Estuario San Francisco. *Fisheries* **2007**, *32* (6), 270−277.
(72) Cloern, J. E. Our evolving conceptual model of the coastal eutrophication problem. *Mar. Ecol.: Prog. Ser.* **2001**, *210*, 223−253.
(73) Dugdale, R.; Wilkerson, F.; Parker, A. E.; Marchi, A.; Taberski, K. River flow and ammonium discharge determine spring phytoplankton blooms in an urbanized estuary. *Estuarine, Coastal Shelf Sci.* **2012**, *115*, 187−199.
(74) Parker, A. E.; Dugdale, R. C.; Wilkerson, F. P. Elevated ammonium concentrations from wastewater discharge depress primary productivity in the Sacramento River and the Northern San Francisco Estuary. *Mar. Pollut. Bull.* **2012**, *64* (3), 574−586.
(75) Seltenrich, N. Remote-sensing applications for environmental health research. *Environ. Health Perspect.* **2014**, *122* (10), A268−A275.
(76) Moore, T. S.; Dowell, M. D.; Bradt, S.; Verdu, A. R. An optical water type framework for selecting and blending retrievals from bio-optical algorithms in lakes and coastal waters. *Remote Sens. Environ.* **2014**, *143*, 97−111.
(77) Kudela, R. M.; Palacios, S. L.; Austerberry, D. C.; Accorsi, E. K.; Guild, L. S.; Torres-Perez, J. Application of hyperspectral remote sensing to cyanobacterial blooms in inland waters. *Remote Sens. Environ.* **2015**, *167*, 196−205.
(78) IOCCG. *Phytoplankton Functional Types from Space*; Sathyendranath, S., Ed.; Reports of the International Ocean Colour Coordinating Group; IOCCG: Dartmouth, Canada, 2014; Vol. No. *15*.
(79) Grimaldo, L. F.; Sommer, T.; Van Ark, N.; Jones, G.; Holland, E.; Moyle, P. B.; Herbold, B.; Smith, P. Factors Affecting Fish Entrainment into Massive Water Diversions in a Tidal Freshwater Estuary: Can Fish Losses be Managed? *North Am. J. Fish. Manag.* **2009**, *29* (5), 1253−1270.
(80) Interagency Ecological Program. *Management, Analysis, A. S. T. An updated conceptual model of Delta Smelt biology: our evolving understanding of an estuarine fish*, 2015.

DOI: 10.1021/acs.est.5b03518
Environ. Sci. Technol. 2016, 50, 573−583